A RESERVOIR ASSESSMENT OF THE SOUTHEAST PART OF OLKARIA DOMES GEOTHERMAL FIELD, KENYA

Felix M. Mwarania

Kenya Electricity Generating Company - KenGen
P.O. Box 785, Naivasha
KENYA
fmwarania@kengen.co.ke

ABSTRACT

The Kenyan rift has great geothermal potential. Fourteen geothermal prospect fields have been identified and about 202 MWe are now generated in one of these fields, Olkaria. This has been a success and, as a result, has called for more drilling to develop Olkaria Domes, a division in the Greater Olkaria area. Appraisal drilling in the Domes field has been completed and the production drilling target of a 140 MWe power plant is at an advanced stage. Warm-up profiles, injection pressure transient tests and discharge results from the wells were used to assess the southeast part of the Domes field. Logging revealed temperatures of over 300°C in the wells at a depth of about 1200 m. The reservoir is two-phase with temperature and pressure following the boiling point curve. The wells have cyclic mass flow but with high enthalpy. The effective permeability of the reservoir varies between 1.1 and 6.1 mD; negative skin is observed in most of the wells.

1. INTRODUCTION

The East African rift valley system runs from the Afar triple junction at the gulf of Eden in the north to Mozambique in the south. In eastern Africa, the rift valley divides into two, the western rift valley and the eastern rift valley. The Kenyan rift is a segment of the eastern Africa rift that extends from Lake Turkana to Lake Natron in northern Tanzania. Geothermal activity is widespread in many parts of the Kenyan rift. These occur as surface manifestations such as fumaroles, geysers, hot grounds and hot springs, among others. Fourteen major geothermal prospects in the rift have been identified but only two have been drilled into (Figure 1). These are the Greater Olkaria and Eburru geothermal fields.

The Greater Olkaria geothermal field is in the southern part of the Kenyan rift. It is located south of Lake Naivasha, approximately 120 km northwest of Nairobi city. The field is divided into seven fields for the sake of development. The different parts are: Olkaria Central, Olkaria East, Olkaria Northeast, Olkaria Northwest, Olkaria Southeast, Olkaria Southwest and Olkaria Domes (Figure 2).

Exploitation of the geothermal resource in the field started in 1981 when Olkaria I power plant, with a 15 MWe turbine, was commissioned. The power plant is in Olkaria East, a part of the Greater Olkaria field. The second and third turbines, each of 15 MWe, were commissioned in 1982 and 1985, respectively. This pioneer power plant is still in place today, producing 45 MWe although it has completed its designed plant life. Olkaria II, which is in Olkaria Northeast, was commissioned in

2003. The plant has been producing 70 MWe but an additional 35 MWe turbine was commissioned in May 2010, increasing the generation capacity to 105 MWe. Olkaria West hosts Olkaria III Independent Power Producer (IPP) power plant. It generates 48 MWe; the first 12 MWe unit was commissioned in 2000 and the second 36 MWe was established in 2009.

Exploration was done in Eburru between 1988 and 1990. Six wells were drilled and plans are under way to put up a 2.5 MWe power plant.

2. BACKGROUND ON GREATER OLKARIA GEOTHERMAL FIELD

2.1 Geophysics

Many seismic studies have been carried out in the Greater Olkaria geothermal area and the results indicate a high level of micro earthquake activity (Lagat, 2004). Resistivity measurements have also shown that the geothermal resource boundaries are controlled by linear structures with NE-SW and NW-SE directions (Figure 3); the resource is confined within the areas with a resistivity value of less than 15 Ωm at an elevation of 1400 m a.s.l (Bw'Obuya and Omenda, 2005).
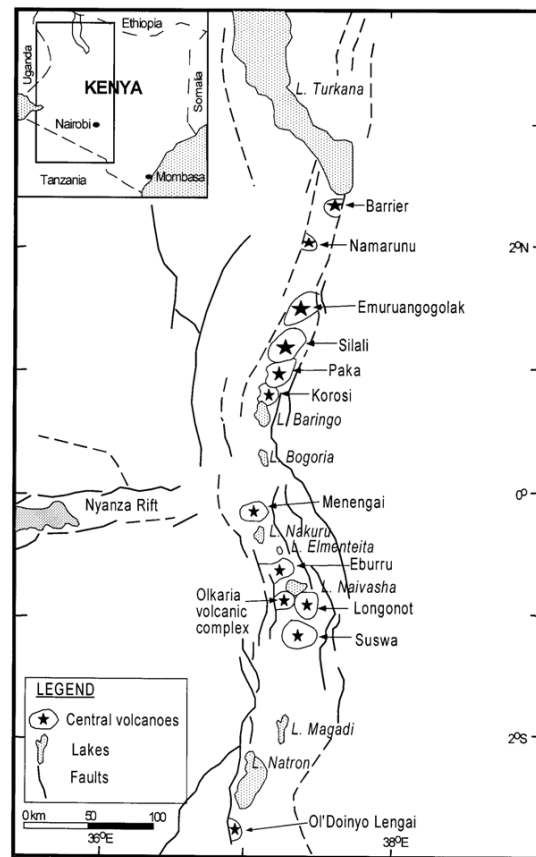

FIGURE 1: Geothermal prospects in the Kenyan rift (Ofwona, 2002)

2.2 Geology

The geothermal field is a part of an old caldera complex that was subsequently cut by N-S normal rifting faults which provided loci for later eruptions of rhyolitic and pumice domes (Ofwona, 2002). The main structures in the caldera complex are: the Ol' Njorowa gorge, the ring structure of volcanic domes, the N-S trending Ololbutot fault and N-S, NNE-SSW, NW-SE and WNW-ESE trending faults
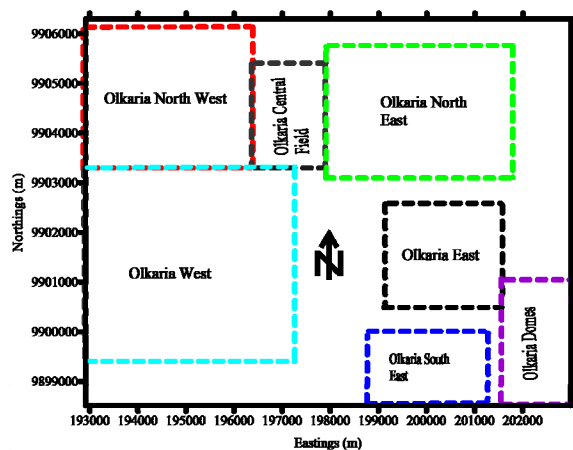

FIGURE 2: Geothermal sectors in the Greater Olkaria geothermal area (Opondo, 2007)
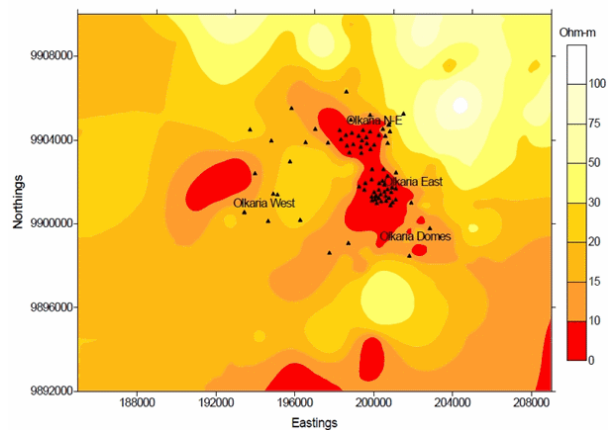

FIGURE 3: Resistivity at 1400 m a.s.l. from TEM measurements (Bw'Obuya and Omenda, 2005)

(Figure 4).   Theses faults are more prominent east, northeast and west of Olkaria although a few are also seen in the Domes, while others are possibly hidden by a pyroclastic cover (Lagat, 2004).

The ring structure is thought to indicate the presence of a buried caldera but might have been produced by the magmatic stresses in the Olkaria magma chamber (Omenda, 1998). Several subsurface faults were encountered during drilling and led to problems like loss of drilling fluids and cement, together with cave-ins.

3. TEMPERATURE AND PRESSURE LOGGING

3.1 Temperature logging

Geothermal energy is the natural heat from the earth, stored in the core, mantle and the crust. The natural heat is transferred from the interior through rocks by conduction. This heats up the meteoric water that percolates into the ground

FIGURE 4: Map showing main geological structures of the Greater Olkaria geothermal system (Lagat, 2004)

through faults and fissures. The heated water rises through other faults and is replaced by more meteoric water; hence, convective heat transfer is enhanced. Finding the temperature of the fluids is an important task in the development of a geothermal system.

Temperature at depth in geothermal systems can be determined by various techniques but the most common is the measurement of the temperature in the wells drilled in the system. This is achieved by running temperature logging tools into the well and later retrieving the logging tools after the data has been recorded. These tools can be electronic or mechanical but accuracy of the data should be paramount. It should be noted that various effects can disturb the temperature in the well such that it may differ from the temperature of the surrounding rock.

The logs show how the measured parameters change as a function of depth. The temperature logs give information on the location of water entries, zones of circulation losses and the recovery trend. This information is a result of disturbances in the well, mainly caused by circulation, injection of water or other heat transfer activities. A fluid loss zone appears in the log as a change in the temperature gradient whereas fluid entry appears as a discontinuous jump in the temperature itself (Stefánsson and Steingrímsson, 1990).

A well may take some time to regain its initial temperature once drilling work is completed. The aquifers may take more time to warm up than the rest of the well but this depends on the properties of the well and its surroundings. Since there is no guarantee that the disturbances in a well will die away once the circulation is stopped, the rock temperature can only be estimated. The rock temperature is estimated from the temperature recovery plots after drilling. The estimation is done by the Horner method using a computer program BERGHITI (Arason et al., 2003) and assumes that conduction is the dominant mechanism of heat transfer. A Horner plot is used for analysing formation temperature at a given depth using a straight line relationship between the temperature at that particular depth and $\ln(\tau)$, where:
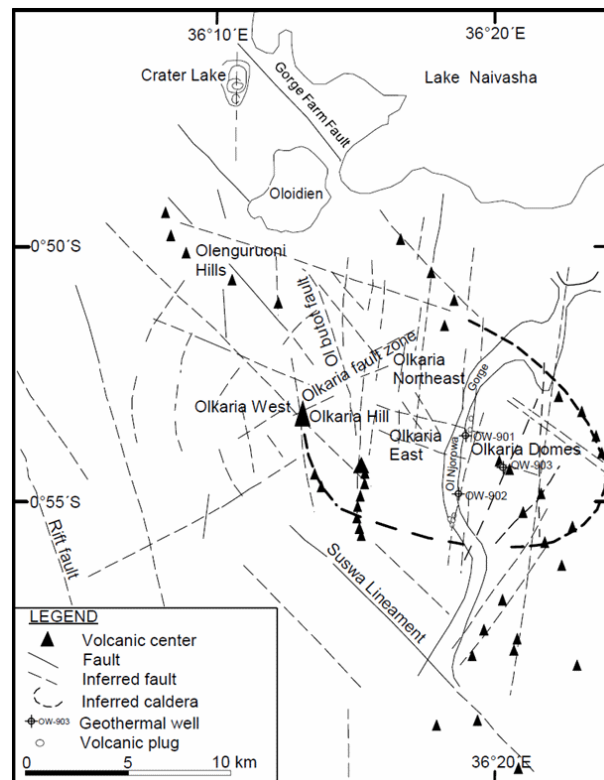
$$\tau = \left(\frac{t_o + \Delta t}{\Delta t}\right) \tag{1}$$

Is the so called Horner time, t_o is the time at which circulation was stopped and Δt is the time passed since circulation stopped.

This shows that $\lim_{\Delta t \to \infty} \ln(\tau) = 0$ and therefore, it is possible to determine the formation temperature from the straight line on a semi logarithmic plot of temperature as a function of the Horner time. The straight line is continued until it intersects the temperature axis at $\ln(\tau) = 0$ (or $\tau = 1$). This procedure can be used at several depths by which a formation temperature profile can be drawn.

3.2 Pressure logging

Pressure is the second most important reservoir parameter after temperature. Pressure drives the flow of fluids in the reservoir. Pressure logging is done to get information on the whole geothermal system rather than the condition or performance of a single well, and to determine the initial reservoir pressure before production; production usually results in a fall in reservoir pressure. However, the skin effect, which is determined by time dependent pressure measurements, is regarded as a property of both the well and the reservoir.

The pressure logs are also used to determine the pivot point in a well during the warm-up period. The pivot point is the point in the well where the pressure in the well represents the reservoir pressure; as the fluid in the well warms up, the pressure profiles will pivot about this point of the pressure profile. This usually occurs at the strongest aquifer in the well and represents a zero point which is difficult to determine later during production (Stefánsson and Steingrímsson, 1990). If the well has two major feed points, the pivot point will appear between them (Grant et al., 1982).

4. INJECTION WELL TESTING

This involves pumping water into a well at a constant rate and measuring the pressure changes in the well as a function of time. The flow is then varied in steps, either increasing or decreasing and the pressure responses are once again monitored. The purpose of this test is to obtain pressure transient data from which the effective reservoir permeability thickness or transmissivity of the reservoir can be calculated, but it describes the ease at which fluid flows through the reservoir. Storativity, which gives information on the storage and the availability of fluid in the reservoir, can be calculated from the data. This is achieved by measuring the pressure at an identified point, preferably the pivot point, which acts as the representative pressure in the reservoir.

If the pressure gauge is located at a wrong level, and in particular if it is set too high, erroneous results are obtained. The oscillatory results obtained are due to the movement of fluids of varying density within the well, causing pressure differences between the levels to vary with time (Grant et al., 1982).

4.1 Theoretical background

One of the most important stages in geothermal reservoir development is to find the response of a given well and reservoir to production or injection. This response helps in evaluating the condition of the well, its flow capacity and the reservoir parameters which cannot be directly known. The parameters include transmissivity, storativity, and wellbore storage and skin among others, and are evaluated using models based on the pressure diffusion equation.

4.1.1 The differential equation

This equation is used to calculate the pressure (p) in a reservoir at a distance (r) from a production or an injection well producing at a given rate (Q) as function of time (t). The Theis solution is the most commonly used solution to the differential equation (Earlougher, 1977; Horne, 1995). The following are assumptions that are used to simplify the situation:

    a) The reservoir is homogenous, isotropic, extends to infinity and has a uniform thickness;
    b) The flow is considered isothermal and radial;
    c) The well penetrates the entire formation thickness;
    d) The formation is completely saturated with single-phase fluid; and
    e) The radius of the wellbore is negligible.

There are three laws that govern in deriving the pressure diffusion equation:

    1) Law of conservation of mass in a given control volume:

$$\text{Mass flow in} - \text{Mass flow out} = \text{Rate of change of mass}$$

$$\rho Q - \left(\rho Q + \frac{\partial(\rho Q)}{\partial r} dr \right) = 2\pi r dr \frac{\partial(\varphi \rho h)}{\partial t}$$

$$-\frac{\partial(\rho Q)}{\partial r} = 2\pi r \frac{\partial(\varphi \rho h)}{\partial t} \tag{2}$$

    2) Law of conservation of momentum, expressed by Darcy´s law:

$$Q = -2\pi r h \frac{k}{\mu} \frac{\partial p}{\partial r} \tag{3}$$

    3) Equation of state of the fluid (fluid compressibility at constant temperature):

$$c_f = \frac{1}{\rho} \left(\frac{\partial \rho}{\partial p} \right) \tag{4}$$

Combining the three equations above results in the pressure diffusion equation given by

$$\frac{1}{r} \frac{\partial}{\partial r} \left(\frac{r \partial p(r,t)}{\partial r} \right) = \frac{\mu c_t}{k} \frac{\partial p(r,t)}{\partial t} = \frac{S}{T} \frac{\partial p(r,t)}{\partial t} \tag{5}$$

where c_t = $\varphi c_f + (1-\varphi)c_r$, the total compressibility;
         c_r = $\frac{1}{1-\varphi} \frac{\partial \varphi}{\partial p}$, the rock compressibility;
         S = $c_t h$;
         T = kh/μ;
         h = Effective reservoir thickness,
         k = Permeability of the rock matrix; and
         μ = Dynamic viscosity of the fluid.

The transmissivity T is large when fluid and pressure responses travel easily through the reservoir, whereas the storativity S describes the storage of the fluid in the reservoir and the amount of the fluid that can be released from the reservoir with a change in pressure.

Theis (Earlougher, 1977; Horne, 1995) proposed an integral solution $p(r, t)$, for a line source, i.e. with a well radius $r_w = 0$:

> *Initial conditions:*
> $p(r,0) = p_i$ for all $r > 0$
>
> *Boundary conditions*:
> $\lim_{r \to \infty} p(r,t) = p_i$ for all $t > 0$
>
> $Q = \frac{2\pi kh}{\mu} \lim_{r \to 0} \left(r \frac{\partial p}{\partial r} \right)$ for all $t > 0$

The Theis solution to the differential equation with the initial and boundary conditions above is given by:

$$p(r,t) = p_i - \frac{Q\mu}{4\pi kh} W\left(\frac{\mu c_t r^2}{4kt}\right) = p_i - \frac{Q}{4\pi T} W\left(\frac{Sr^2}{4Tt}\right) \tag{6}$$

where $W(u) = -Ei(-u) = \int_u^{\infty} \frac{e^{-x}}{x} dx$ is the well function or the exponential integral function.

For small values of $u = \frac{Sr^2}{4Tt}$, i.e $u < 0.01$, $W(u) \approx -\ln(u) - \gamma \approx -\ln(u) - 0.5772$ where γ is the Euler constant. Therefore, if:

$$t > 25 \frac{Sr^2}{T} = 25 \frac{\mu c_t r^2}{k}$$

the Theis solution becomes:

$$p(r,t) = p_i + \frac{2.303Q}{4\pi T}\left[\log\left(\frac{Sr^2}{4Tt}\right) + \frac{\gamma}{2.303}\right]$$

and this can be further simplified to:

$$p(r,t) = p_i - \frac{2.303Q}{4\pi T} \log\left(\frac{2.246T}{Sr^2} t\right) \tag{7}$$

Pressure transmission in the reservoir does not take place uniformly since it is affected by local heterogeneities. There is a zone surrounding the well that can be invaded by mud filtrate or cement during drilling, or the surroundings close to the well can be fractured. This zone has a different permeability than the reservoir at large and acts like a ''skin'' causing an extra pressure drop (Δp_s):

$$\Delta p_s = \frac{Q}{2\pi T} s \tag{8}$$

The degree of damage or improvement is expressed in terms of a ''skin factor'', s, which is positive for damage and negative for improvement. The skin effect due to a damaged zone of radius r_s and reduced permeability k_s can be calculated from:

$$s = \left(\frac{k}{k_s} - 1\right) \ln\left(\frac{r_s}{r_w}\right) \tag{9}$$

Since the skin has the same effect as changing the effective radius of the well, the effective well radius r_{weff}, is given by:

$$r_{weff} = r_w e^{-s} \tag{10}$$

If the skin zone permeability k_s is higher than that of the reservoir, the skin effect in Equation 9 becomes negative. The effective wellbore radius in this case, given by Equation 10, will be greater than the actual radius and the pressure distribution would appear as in Figure 5.

In a pumping well with skin, the total pressure change is given by:

$$\Delta p = p_i - p(r_w, t) = \frac{Q}{4\pi T}\left[W\left(\frac{Sr_w^2}{4Tt}\right) + 2s\right]$$

$$\approx \frac{Q}{4\pi T}\left[\ln\left(\frac{4Tt}{Sr_w^2}\right) - \gamma + 2s\right]$$

which further reduces to:

$$\Delta p \approx \frac{2.303Q}{4\pi T}\left[\log(t) + \log\left(\frac{T}{Sr_w^2}\right) + 0.3514 + 0.8686s\right] \tag{11}$$

4.1.2 Semi logarithmic well test analysis

A plot of the Theis solution on a lin-log graph, i.e. for Δp vs. log t, gives a semi-log straight line response for the infinite acting radial flow period of the well, and is referred to as semi log analysis. Transmissivity is found when the slope m is identified from the asymptotic straight line obtained from the plot. Dynamic viscosity is obtained from steam tables if the reservoir temperature and pressure are known.

$$m = \frac{2.303Q}{4\pi T} = \frac{2.303\mu Q}{4\pi kh} \tag{12}$$

where m is measured in (Pa/log cycle)

Storativity can be obtained when transmissivity has been found, assuming that the initial pressure p_i is known and that there is no skin effect, using:

$$S = 2.246T\frac{t}{r^2}10^{\frac{-\Delta p}{m}} \tag{13}$$

where $\Delta p = p_i - p(r, t)$

The semi-log analysis is based on the interpretation of the semi log straight line response that represents the infinite acting radial flow behaviour of the well. However, an actual wellbore has a finite volume, and it becomes necessary to determine the duration of the wellbore storage effect or the time at which the semi-log straight line begins. On a log-log plot of (Δp) vs. (t), a characteristic unit slope identifies the wellbore storage effect.

"Wellbore storage disguises the reservoir response in the beginning, making interpretation difficult. However, the storage effect gets depleted after approximately 1½ log cycles during which the response undergoes a transition between the wellbore and the reservoir response. Once the wellbore storage
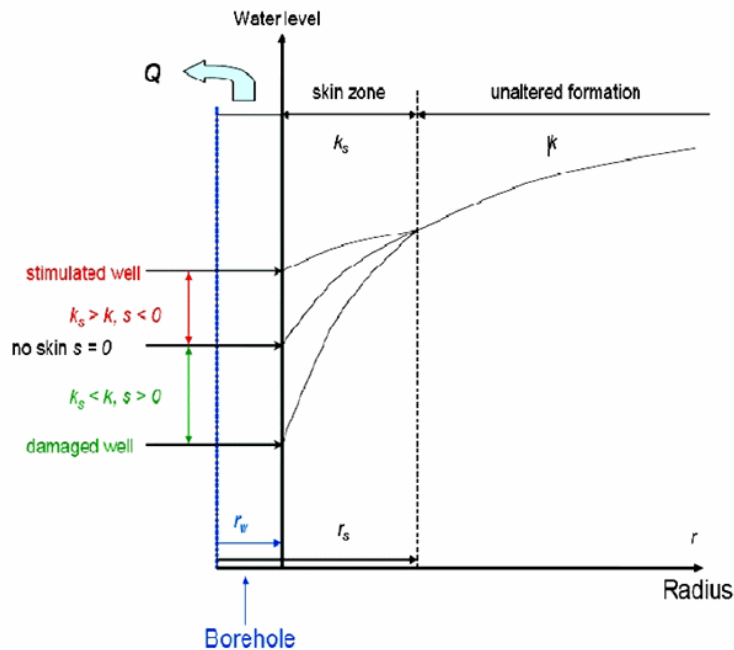
FIGURE 5: Pressure changes in the vicinity of a well
due to the skin (Jónsson, 2010)

and the transition effects are over, the wellbore pressure transient reflects the pressure transmission of an infinite reservoir. As time proceeds, this response is characteristic of conditions farther and farther away from the wellbore. At very late time, the response is affected by the influence of the reservoir boundaries, but prior to those late times the pressure response does not ''see'' the reservoir boundaries, and the reservoir acts as if it were infinite in extent. This intermediate time response between the early wellbore-dominated response and the late boundary-dominated response is called the "infinite acting period" (Horne, 1995) and is characterised by a straight line on a semi-log plot of pressure versus time.

5. PRODUCTION CAPACITY ASSESSMENT

5.1 Theoretical background

Once a geothermal well has been drilled and given time to warm up, the well production capacity is anticipated and may be estimated. This, however, is not always correct. Thus, the well has to be discharged to get the exact production in terms of wellhead pressure (WHP) and the steam flow rate. The electric power output can then be calculated from these parameters. The well is opened to the atmosphere to eject solid matter, either from drilling material such as cuttings and mud or newly broken rock from the formation. The well discharges later into a silencer which acts as a steam-water separator at atmospheric pressure. The water collected is measured as it flows from the silencer over a V-notch weir, but steam rises and escapes. Several measurements for different flow rates are achieved by letting the steam-water mixture flow through different sizes of lip pressure pipes into the silencer. The parameters measured are:

- Wellhead pressure;
- Lip pressure; and
- Height of the water in the V-notch weir.

Russell-James´s formula relates the mass flow rate, discharge pipe area, enthalpy and lip pressure (Grant et al., 1982):

$$Q_t = \frac{k \times A \times P_{lip}^{0.96}}{H_t^{1.102}} \tag{14}$$

where k is a constant depending on the units, Q_t is the total mass flow rate in kg/s and A is the cross section area of the lip pipe in cm^2.

The total mass flow rate obtained from this method can be related to the water flow rate measured at the V-notch weir after separation in the silencer:

$$Q_t = Q_w \frac{H_s - H_w}{H_s - H_t} \qquad (15)$$

For atmospheric conditions, H_s = 2676 kJ/kg and H_w=419 kJ/kg and thus Equation15 simplifies to:

$$Q_t = Q_w \frac{2256}{2676 - H_t} \qquad (16)$$

Combining Equations 14 and 16 gives the solution for H_t, the total fluid enthalpy, the only unknown in the Equation 17:

$$Q_w \frac{2256}{2676 - H_t} = \frac{k \times A \times P_{lip}^{0.96}}{H_t^{1.102}} \qquad (17)$$

6. RESULTS OF THE SOUTHEAST DOMES FIELD ASSESSMENT

Over twenty wells have been drilled in Olkaria Domes field over the past few years. Appraisal drilling of six wells started in June 2007 but intense production well drilling activity was in progress in October 2010, when this paper was written. The wells, some vertical while others are directional, were drilled to 3000 m measured depth. The directional wells were designed with a directional profile from a kick off point (KOP) of 400 m. Directional drilling has increased well outputs in the Domes, possibly because the wells intercept more fractures and faults in the area. Olkaria IV power plant, which is expected to generate 140 MWe, will be situated in this field. Four wells were considered for analysis in this report. They are OW-909A, OW-915A, OW-912 and OW-911A.

6.1 Temperature and pressure logging analysis

Logging in the Olkaria Domes was done using Kuster mechanical tools when the drill rig reached the final depth in a well. Logging in geothermal wells is done by stopping the logging tools at intervals of 50 m for a total duration of 4 minutes.

6.1.1 Interpretation of temperature and pressure logs

Figures 6 to 9 show temperature and pressure plots for the four Domes wells under consideration. From the logging data, temperature plots were made and these helped locate aquifers in the wells. This was done with the content in Table 1 in mind. The computer program BOILCURV (Arason et al., 2003) was used to estimate the boiling conditions. Various feed zones were noted at several depths on the four temperature plots.

In OW-909A (Figure 6), the feed zones are located at around 1600 m, 2100 m and at the well's bottom. The aquifer at 2100 m dominates the well. The latest profile is almost isothermal for depths between 1200 and 2200 m and boiling was observed in the well. Pressure profiles show the pivot point at around 1900 m. It can be observed that the latest pressure profile follows the estimated formation pressure with a few exceptions and the wellhead pressure in the well is around 25 bar-a. It should be noted that about seven temperature and pressure loggings were done during warm-up but two pressure logs failed.

TABLE 1: Olkaria Domes well properties

Well no.	Orientation	Drilled depth (m)	Casing depth (m)
OW-915A	deviated	2997	989
OW-909A	deviated	2960	855
OW-911A	deviated	3000	902
OW-912	vertical	3010	849

The temperature profile done immediately after drilling in OW-915A (Figure 7) showed feed zones located at 1100 m and 1800 m depth, expressed as a change in the temperature gradient. The kicks were observed in other profiles as the well heated up, confirming the feed zones. The profile after 13 hours of injection tests also indicated some permeability at the well bottom and, thus, a feed zone at that point. The last profile showed boiling conditions for depths between 1000 m and 1800 m. The pressure pivot point is located at around 2000 m depth.

In Figure 8, one can see aquifers located at 1000, 2400, 2700 and 2900 m depth in well OW-912. The logs identified 2900 m as the deepest water loss zone in the well. Boiling conditions between 1000 and 1600 m were also evident in the well. Considering the last three profiles, the pivot point is located at around 1500 m depth.

Lastly, in OW-911A (Figure 9) heating in the well was not as rapid as in the other three Domes wells but convective heating was evident from the temperature profiles. The last log showed almost isothermal temperatures but far from boiling conditions, implying the presence of liquid in the well. The computer program PREDYP (Arason et al., 2003) was used to calculate pressure in static water columns with known temperatures. Temperature plots showed a water loss zone at around 900 m but the major loss zone is at around 2500 m depth. Pressure plots do not show a clear pivot point in the well.   The pressure log after injection showed pressure build-up in the well, predicting low permeability.
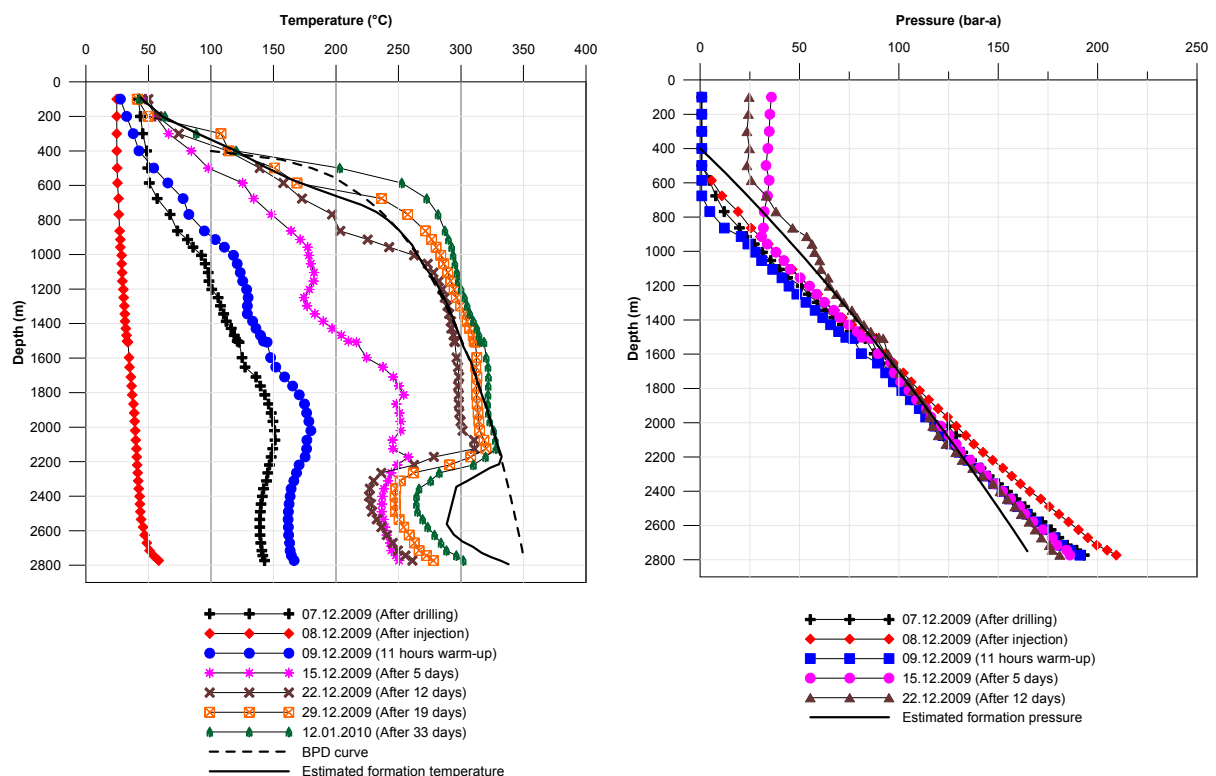

FIGURE 6: OW-909A temperature profiles (left) and pressure profiles (right)
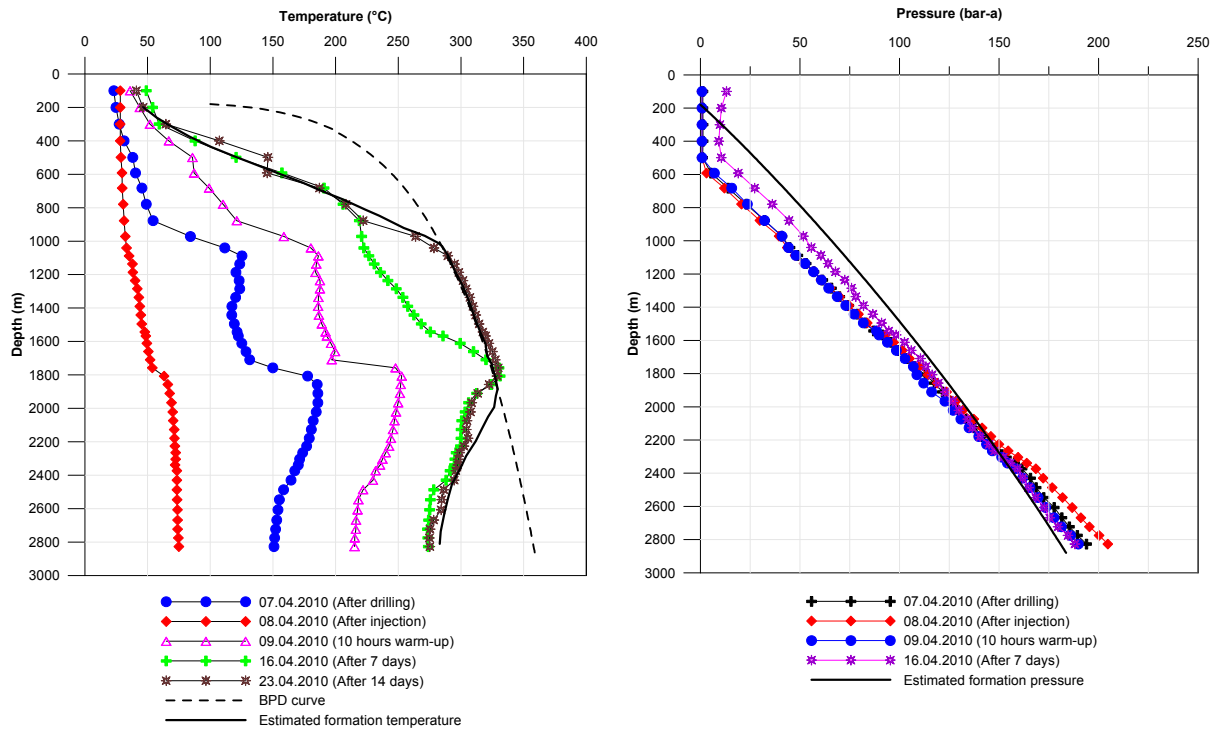
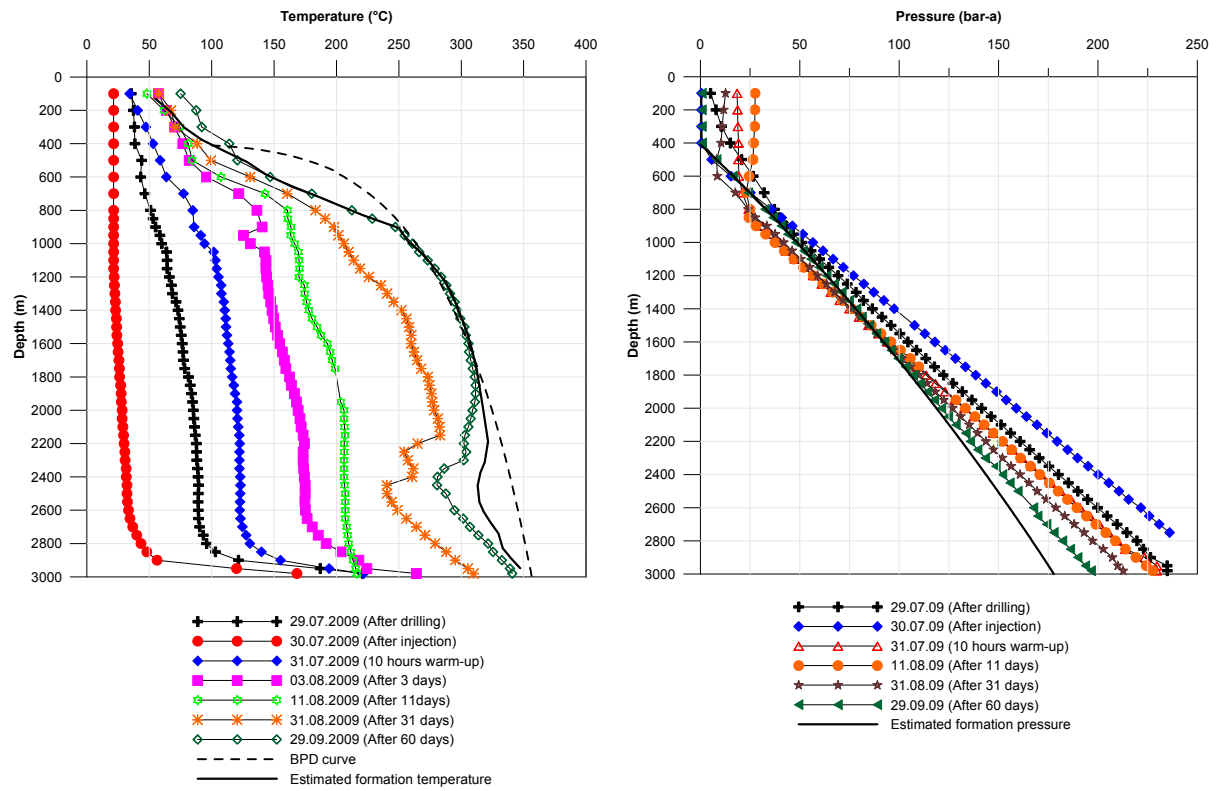FIGURE 7: OW-915A temperature profiles (left) and pressure profiles (right)

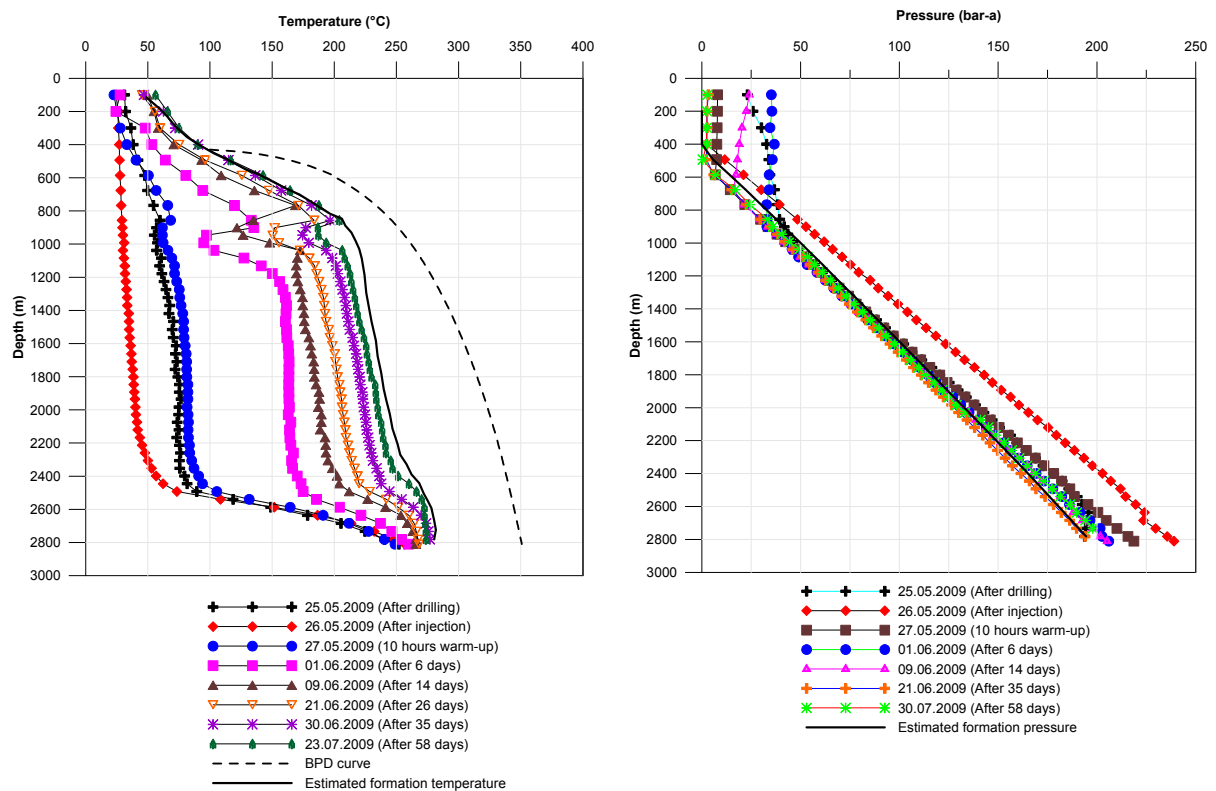FIGURE 8: OW-912 temperature profiles (left) and pressure profiles (right)

FIGURE 9: OW-911A temperature profiles (left) and pressure profiles (right)

It should be noted that, for the four wells, the temperature decreased gradually from around 800 m up to the surface. This could indicate conductive heat transfer through the formation and thus the plots could closely represent the formation temperature. In addition, the temperature inversion observed in OW-909A, OW-915A and OW-912 plots at the well bottom, might be due to cooling effects of the drilling fluids. Drilling processes or any subsequent cold water injection cools the wellbores by the flow of water or drilling mud. After this ceases, the wells warm up either slowly or quickly to the final temperature. The temperature inversion can be checked by logging a well at a later date but it may be assumed that, after a long heating period, temperature disturbances will die away and the temperature will align itself with the true formation temperature.

6.1.2 Temperature and pressure cross-sections

A model of the area hosting the wells under consideration can be realised best by drawing horizontal cross-sections at different elevations and vertical cross-sections in different directions. It should be noted that the contours in both horizontal and vertical cross-sections were plotted using the estimated formation data (temperature in °C and pressure in bar-a) to represent reservoir conditions.

Figure 10 shows temperature and pressure distribution at 1000 metres above sea level (m a.s.l.). The hottest zone is in OW-909A and the coldest in OW-911A. It can be observed from the pressure distribution that the low-pressure zone in OW-911A coincides well with low temperature. Low pressure potential indicates areas of rapid heat and mass sink (downflow of fluid and heat loss) while the high potential area indicates zones of fluid and heat inflow/upflow (Ofwona, 2002). The topography of the terrain also plays a role in the pressure distribution.

Figure 11 shows the location of the Domes wells and vertical cross-sections of temperature in the N-S and E-W directions. From the N-S section, the three wells seem to have penetrated the hottest part of the reservoir. The temperature contours are almost horizontal and not much can be realised from the
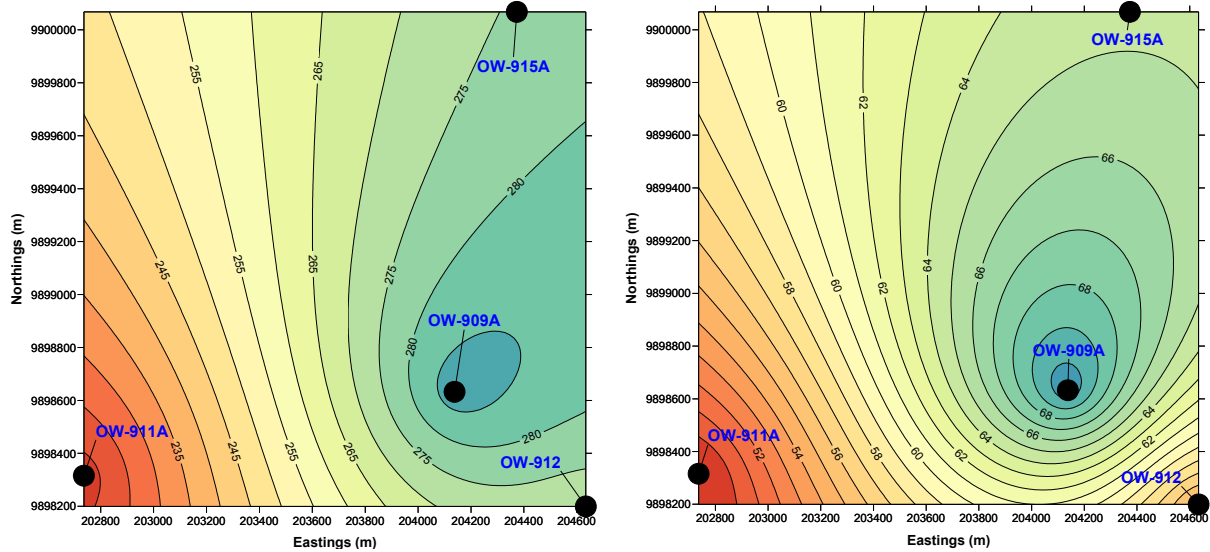
FIGURE 10: Distribution of temperature (left; °C) and pressure (right; bar), at 1000 m a.s.l.

section unless more wells are included. However, a hot plume was observed in well OW-909A. From the E-W section, again a plume was observed in OW-909A. The cross-section shows heat flows from the area around OW-909A towards the west (left) and east, but the eastern side is not dominant unless temperature extrapolation is done. Note that the numbers on the contours in Figure 11 (left) give the approximate altitude in m a.s.l.

6.2 Injection testing and analysis

6.2.1 Injection test

The wells under consideration were all drilled at different times within a year. The same injection test procedure was used for all the wells. This involved stationing a temperature/pressure logging tool at an identified depth in a well and then injecting cold water into the well at different pumping rates. The initial flow rate into the well was 0 L/s before pumping began with 16.7 L/s. This lasted for four hours before the pump rate was increased to 21.7 L/s, 26.7 L/s and 31.7 L/s, respectively. The second, third and fourth pumping periods lasted three hours each.
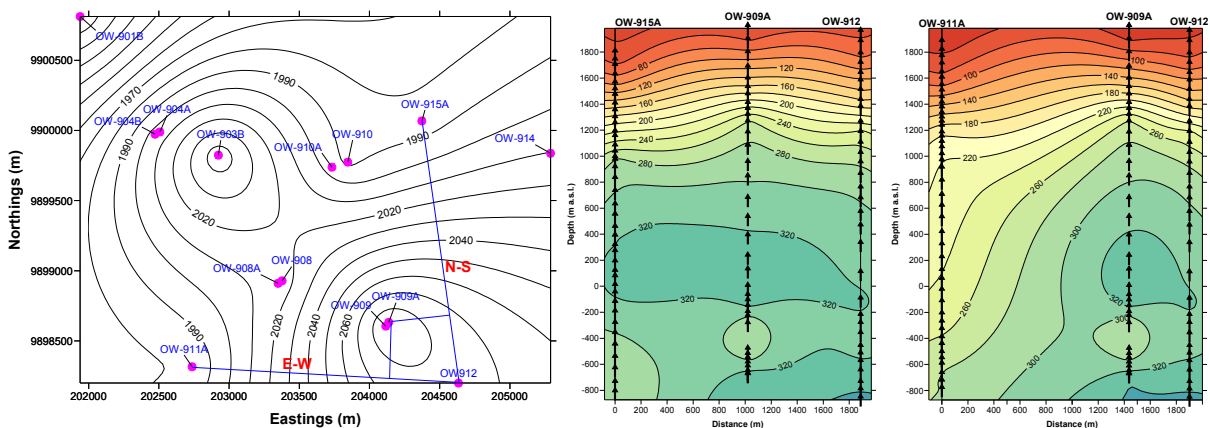

FIGURE 11: Domes field. Location of the wells (left), N-S temperature cross-section (centre; °C);
and E-W temperature cross-section (right; °C)

6.2.2 Injection test analysis

Well test analysis offers a rapid way to perform initial assessment of a geothermal field. A computer program WELLTESTER (Júlíusson et al., 2008), based on non-linear regression, was used in the analysis of the data. A non linear regression analysis was performed to find the parameters that best fit the data gathered. Many attempts were made using the derivative plot to compare with the trend of different boundary conditions in order to come up with an appropriate model. The details on the model selected for the four wells were:

- The reservoir is homogenous;
- Constant pressure boundary; and
- Constant skin and wellbore storage.

Only the steps that fit best in the model are presented. Log-linear, log-log scale and the derivative of the pressure response multiplied by the time passed since the beginning for the selected steps are shown for each well. The parameters achieved are the best estimates from the non linear regression analysis.

OW-909A: The pressure tool was stationed at 2490 m depth in this well. Only two steps fit best in the model. Figures 12 and 13 are the plots from the two steps. The parameters estimated from the steps are tabulated in Table 2.
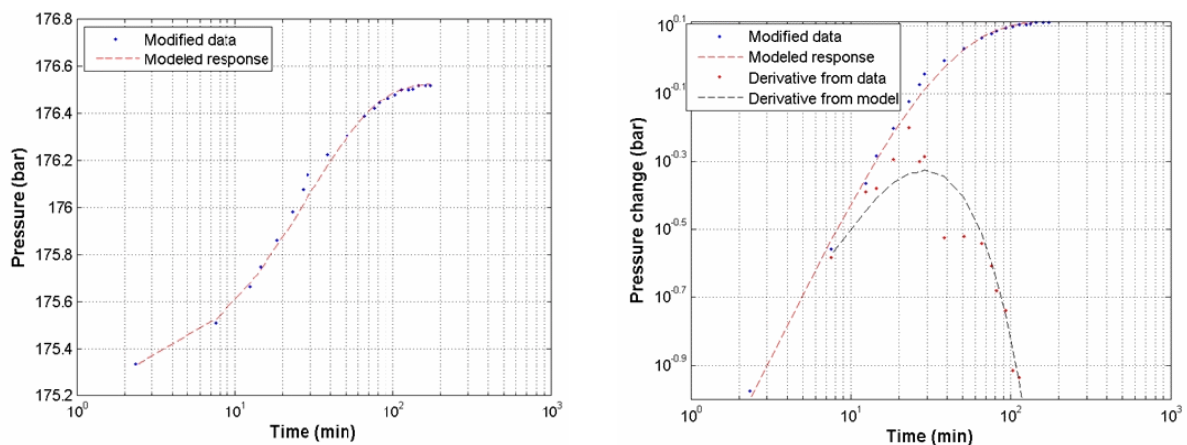
FIGURE 12: OW-909A, fit between model and selected data for step 3 on a log-linear scale (left) and on a log-log scale (right)
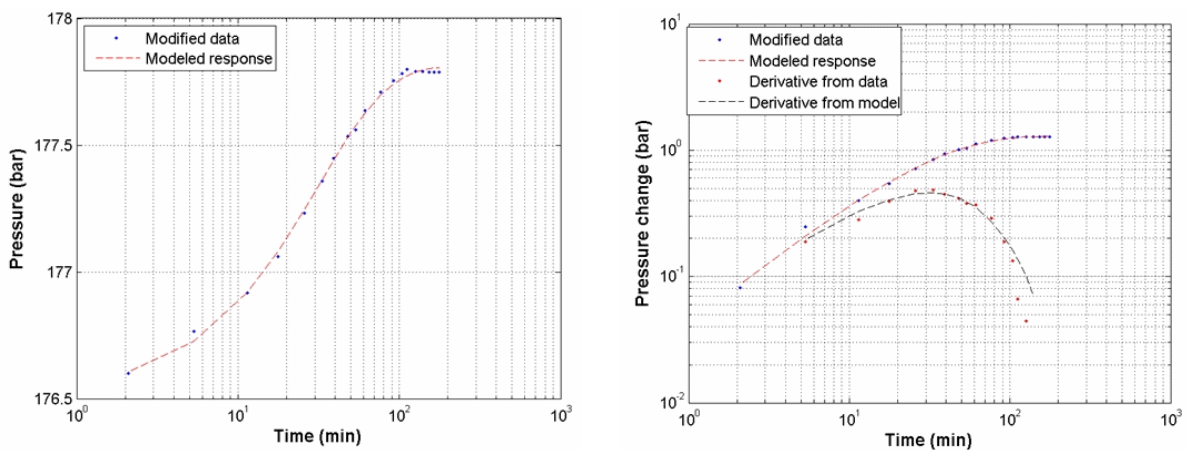
FIGURE 13: OW-909A, fit between model and selected data for step 4 on a log-linear scale (left) and on a log-log scale (right)

TABLE 2: Summary of non-linear regression parameters obtained
from injection data in OW-909A

	Transmissivity (m³/(Pa·s))	Storativity (m³/(Pa·m²))	Skin -	Permeability (mD)	Injectivity (model) ((L/s)/bar)	Injectivity (data) ((L/s)/bar)
Step 3	1.5×10^{-8}	4.5×10^{-8}	-2.1	1.1	3.9	3.9
Step 4	3.0×10^{-8}	3.7×10^{-8}	-1.1	2.7	3.9	3.9

OW-915A: The pressure tool was stationed at 2490 m depth. Only one step fits best in the model.
Figure 14 shows the plot from that step. The parameters estimated from the step are given in Table 3.
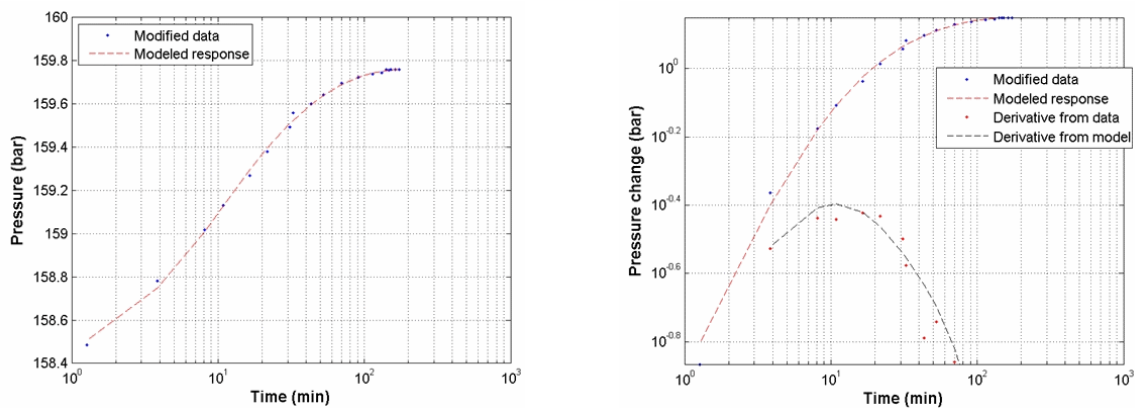
FIGURE 14: OW-915A, fit between model and selected data for step 2 on a log-linear scale (left)
and on a log-log scale (right)

TABLE 3: Summary of non-linear regression parameters obtained
from injection data in OW-915A

	Transmissivity (m³/(Pa·s))	Storativity (m³/(Pa·m²))	Skin -	Permeability (mD)	Injectivity (model) ((L/s)/bar)	Injectivity (data) ((L/s)/bar)
Step 2	2.9×10^{-8}	4.2×10^{-8}	-1.5	2.4	3.5	3.5

OW-912: The pressure tool was stationed at 2600 m depth. Only one step fits best in the model.
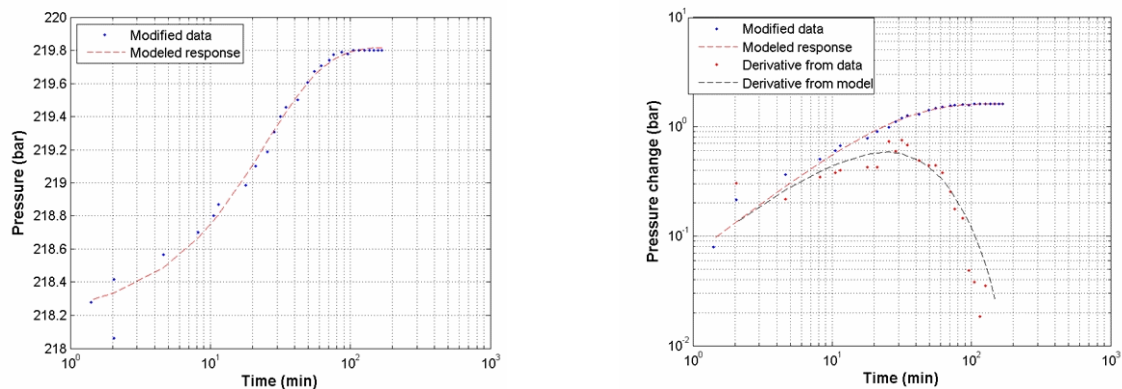Figure 15 shows the plot from the step. The parameters estimated from the step are given in Table 4.

FIGURE 15: OW-912, fit between model and selected data for step 4 on a log-linear scale (left)
and on a log-log scale (right)

TABLE 4: Summary of non-linear regression parameters obtained from injection data in OW-912

	Transmissivity (m³/(Pa·s))	Storativity (m³/(Pa·m²))	Skin -	Permeability (mD)	Injectivity (model) ((L/s)/bar)	Injectivity (data) ((L/s)/bar)
Step 4	2.8×10^{-8}	1.6×10^{-8}	-0.7	6.1	3.1	3.1

OW-911A: The pressure tool was stationed at 2445 m depth. Only two steps fit best in the model. Figures 16 and 17 are the plots from these two steps. The parameters estimated from the steps are given in Table 5.
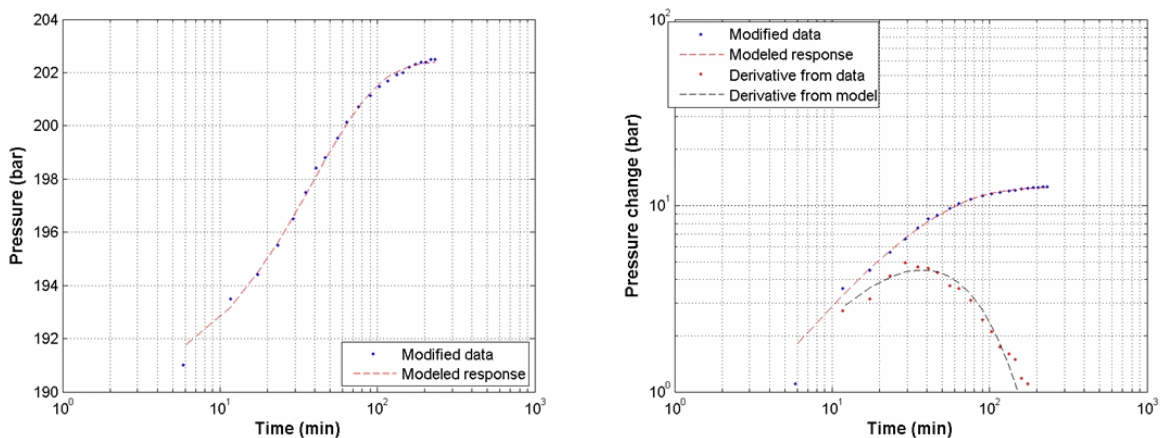

FIGURE 16: OW-911A, fit between model and selected data for step 1 on a log-linear scale (left) and on a log-log scale (right)
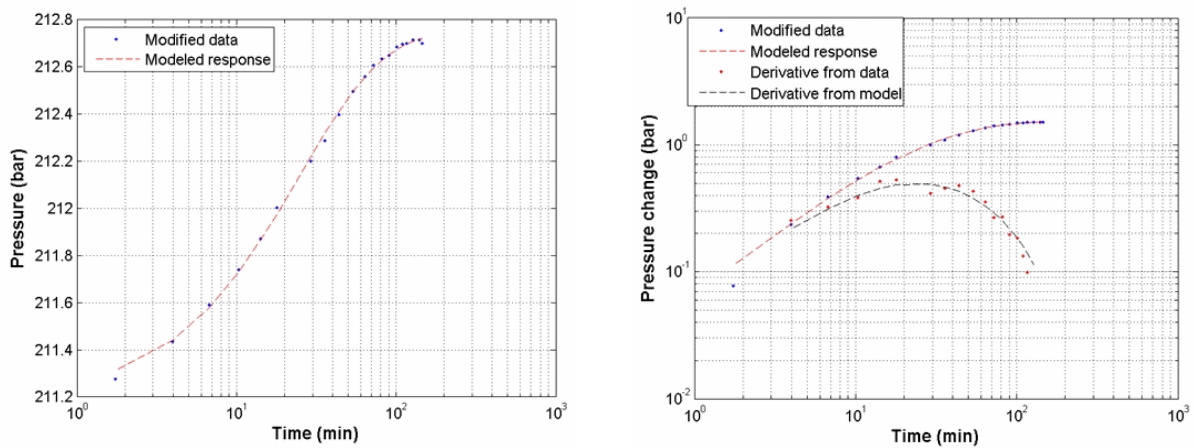
FIGURE 17: OW-911A, fit between model and selected data for step 4 on a log-linear scale (left) and on a log-log scale (right)

TABLE 5: Summary of non-linear regression parameters obtained from injection data in OW-911A

	Transmissivity (m³/(Pa·s))	Storativity (m³/(Pa·m²))	Skin -	Permeability (mD)	Injectivity (model) ((L/s)/bar)	Injectivity (data) ((L/s)/bar)
Step 1	1.5×10^{-8}	4.4×10^{-8}	2.1	1.6	1.3	1.3
Step 4	3.3×10^{-8}	4.7×10^{-8}	-0.3	3.4	3.3	2.8

Working with the data was tedious and many attempts had to be made. It was suspected that there might be a time and pressure datum shift during data collection. This meant that, at the indicated time, the actual pressure might not have been the one recorded at that time. This is because the pressure transducers take time to stabilize. For this reason, the actual time for the early data might have been different; the error introduced is significant when a logarithmic plot is made. Interpretation of the plots was, therefore, impaired.

The transmissivity describes the ability of the reservoir to transmit fluid. The values obtained were on the order of 10^{-8} m^3/ (Pa·s) and were within the range obtained from the wells directly opposite in the Domes field (Kariuki, 2003). On the other hand, storativity describes the volume of fluid the reservoir is capable of storing and releasing per unit area of aquifer, per unit pressure increase. The values obtained were lower than those obtained from the opposite side of the field.

Permeability is a key factor in the flow potential of a well. It enhances natural convection in the geothermal system. In addition, wells with good permeability have flow paths that connect the wells to the reservoir. The reservoir thickness obtained from the selected steps ranged from 430 to 1530 m. The corresponding permeability values ranged from 1.1 to 6.1 mD.

The injectivity index (*II*) was used to estimate the well's productivity prior to completion. The index is useful in deciding what equipment will be needed for discharge tests. It is defined as the change in the injection flow (ΔQ) divided by the change in the stabilized reservoir pressure (ΔP):

$$II = \frac{\Delta Q}{\Delta P} \tag{18}$$

The injectivity index values obtained ranged from 1.3 (L/s)/bar to 3.9 (L/s)/bar. The values from the data and the model matched well except for one of the selected steps. This is because WELLTESTER picks pressure values from the model for calculating the index and these values might be higher or lower than those from the input data.

6.3 Production capacity testing and analysis

Wells in Olkaria Domes were discharge tested after a warm-up period, which is normally one month but in some cases lasted longer.

6.3.1 Well OW-911A

This well had to be pressurised with air to initiate the flow since it had no wellhead pressure; starting the discharge by simply opening the wellhead control valve was not possible. However, suddenly opening the wellhead control valve after pressurising with air permitted the discharge of the compressed air followed by boiling geothermal fluid.

Well OW-911A was then tested with three lip pipes (Figure 18): 8", 6" and 5" but could not sustain discharge on the 5" lip pipe. Two attempts to discharge the well through the pipe failed. The wellhead pressure was lower than 5 bar-a for all the lip pipes; consequently, this well cannot be used in eletricity production for commercial purposes since the pressure is lower than the operation pressure for the Olkaria power plant turbines. The amount of steam flow from the well is too low compared to the water flow, confirming the temperature logging plots which showed that the well was far from boiling. Low enthalpies were also achieved, being near that of liquid water at the pressure and temperature of the main feed point (Figure 18). The well seems to be tapping a liquid-dominated geothermal reservoir.
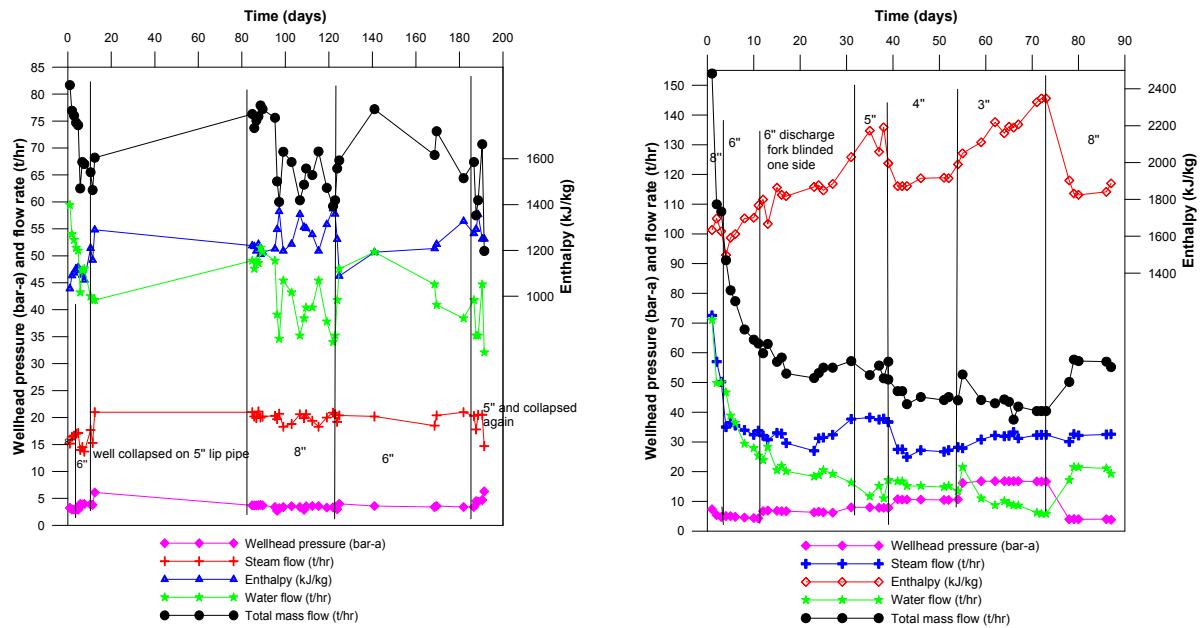
FIGURE 18: Discharge history of OW-911A (left) and OW-912 (right)

6.3.2 Well OW-912

Like OW-911A, this well had to be pressurised to initiate discharge. Well OW-912 had a very high mass flow upon opening and had to be discharged through two separators. This, however, could not be sustained and the discharge

TABLE 6: OW-912 discharge output summary

Lip pipe (inch)	Whp (bar-a)	Mass flow (t/hr)	Steam flow (t/hr)	Enthalpy (kg/kJ)
8	4	55.5	32	1856
6	6.6	56.2	31.2	1825
5	7.9	54.1	37.4	2072
4	10.6	45	27	1907
3	15.7	42.8	31.7	2201

gear had to be blinded on one side (Figure 18) to ensure that reasonable testing could continue. This was done after twelve days of discharge testing. The well was tested with five different lip pressure pipes and sustained discharge in all cases. An average of the output data per lip pipe was computed and is shown in Table 6. The data included in the table for analysis is only for the part of the test after the discharge gear was blinded on one side. The values of the flow rate are averages while those of the enthalpy are weighted averages.

6.3.3 Well OW-909A

Initial self-sustaining discharge was possible due to the presence of wellhead pressure. Table 7 shows average values of flow rate and weighted enthalpy values achieved per lip pipe during the tests. The

TABLE 7: OW-909A discharge output summary

Lip pipe (inch)	Whp (bar-a)	Mass flow (t/hr)	Steam flow (t/hr)	Enthalpy (kg/kJ)
8	7.1	140.1	79.1	1777
6	7.4	112.6	63.5	1828
5	8.5	112.0	65.0	1864
4	11.6	94.4	46.0	1670

well sustained discharge through four different lip pressure pipes with stable wellhead pressures above 5 bar-a achieved. From Figure 19, it can be seen that the wellhead pressure is almost stable for each pipe; the enthalpy and steam flow rate cycles were sufficient for all lip pipes during the entire discharge test period. It was also generally observed that the enthalpy varied with the steam flow rate for most parts of the discharge test.

FIGURE 19: Discharge history, a) OW-909A; b) OW-915A

6.3.4 Well OW-915A

Here, self initial discharge was possible like in OW-909A. Initial discharge (Figure 19) showed high mass and water flow rate, which was later reduced; this was assumed to be a wellbore storage effect.

TABLE 8: OW-915A discharge output summary

Lip pipe (inch)	Whp (bar-a)	Mass flow (t/hr)	Steam flow (t/hr)	Enthalpy (kg/kJ)
8	7.7	126.9	87.8	2152
6	7.6	111.2	88.7	2322
5	9.9	120.2	100.2	2399
4	13.8	103.7	89.3	2457

However, this reduction was not as massive as in OW-912. For almost constant wellhead pressure, enthalpy and flow rate cycles were achieved for most of the test period but with higher averages and weighted averages (Table 8).

6.3.5 Characteristic curve

The characteristic or output curve is used to relate the total mass flow rate of a well to its wellhead pressure. The total mass flow rate results obtained from the output tests at different throttle conditions should form a smooth curve when plotted against flowing wellhead pressure. This helps to estimate the amount of steam and brine available from a well at a given point in time; these estimates are then used to set design and operating parameters for a geothermal plant.

From Figure 20, it can be observed that OW-915A gave the highest mass flow at all wellhead pressures. OW-909A has a constant mass flow for wellhead pressure below 8.5 bar-a. Well OW-911A could not sustain discharge at the required 5 bar-a wellhead pressure and, thus, was not included in the plot.

7. DISCUSSION AND CONCLUSIONS

The southeast part of Olkaria Domes geothermal field can be classified as a high-temperature and a high-enthalpy field. According to Axelsson (2008), a geothermal field is termed as high-temperature field with high enthalpy if the reservoir temperature at 1000 m depth is above 200°C and the reservoir fluid enthalpy is greater than 800 kJ/kg. Temperature plots have shown higher temperatures than 200°C are achieved in the wells at 1000 m depth and the enthalpy is higher than 800 kJ/kg. The part of the Domes field under consideration gave very different results from the opposite side of the field. The part of the field hosting OW-901, OW-902 and OW-903, the Domes exploration wells, showed fluids with low enthalpy at very low wellhead pressure (Odeny, 1999).
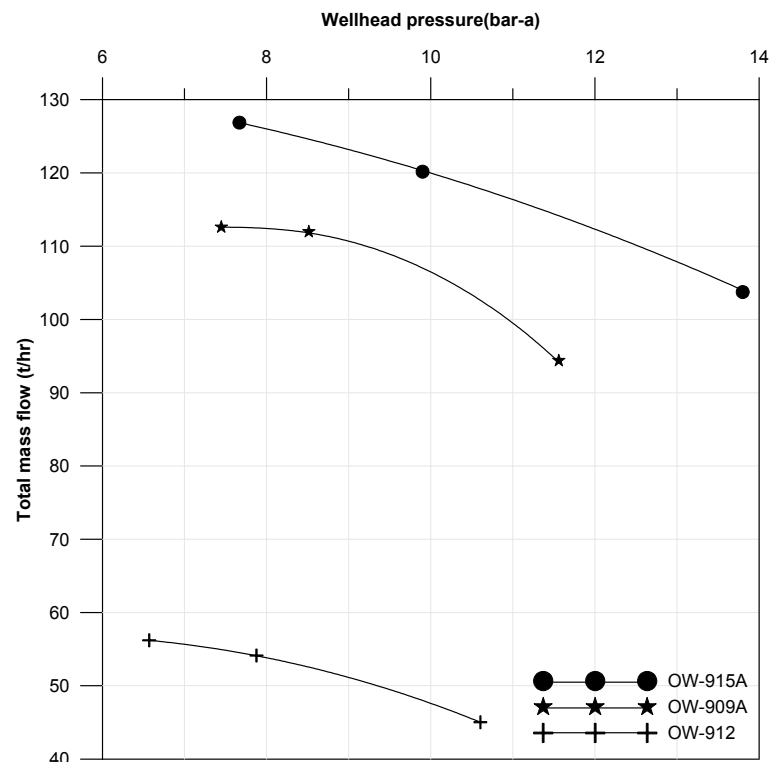

FIGURE 20: The output curves for the Domes wells

It can be assumed that part of the Domes field is in two-phase conditions since steam and water co-exist and 75%, of the representative wells considered, obey the saturation relationship for the local fluid for most parts of the well. However, a clearer picture of the field could be revealed if more or all wells were included in the study. In addition, temperature and pressure logging should be done at a later date to find out if the inversion in the wells is due to cooling through drilling fluids or to cold inflow into the field at that particular depth.

The temperature logs also show clearly that the wells in the field are fed from multiple feed points. This is supported by the cyclic behaviour observed in the wells. Grant (1979) explains that cycling in wells indicates the presence of more than one feed zone. The instability is dependent on the pressure difference variation between the two feed points as the fluid in the well oscillates between liquid and two-phase conditions.

The log-log plots for the steps from the four wells that fit best to the model show a constant boundary effect. The effective permeability obtained from the wells varied from 1.1 to 6.1 mD. According to Odeny (1999), the Olkaria field permeability average values were 7.5 and 4.0 mD for steam and liquid zones, respectively. The values obtained from the southeast Domes wells were within a similar range.

In summary:

1. The southeast part of the Domes area is a high-temperature and high-enthalpy field.
2. The field is in two-phase conditions, with the temperature and pressure following the boiling point curve.
3. The field has permeability between 1.1 and 6.1 mD.

ACKNOWLEDGEMENTS

I would like to express my gratitude to Dr. Ingvar B. Fridleifsson and Mr. Lúdvík S. Georgsson for the chance to study and greatly appreciate the support from the UNU-GTP programme. I am also grateful to my employer KenGen for granting me study leave and providing data for use in this project.

I appreciate, Ms. Thórhildur Ísberg, Ms. Dorthe H. Holme, Mr. Markús A.G. Wilde and Mr. Ingimar G. Haraldsson for their great assistance during my study and stay in Iceland. Great thanks go to my supervisors, Mr. Páll Jónsson, Dr. Svanbjörg H. Haraldsdóttir and Ms. Saeunn Halldórsdóttir, for their advice and guidance throughout the study. They shared a lot of knowledge with me. To my fellow students: great moments were spent together.

Thanks to Tiberius Masese and Wilson Omenda, among other KenGen staff, who worked tirelessly to ensure I got all the required data.

DEDICATION

I dedicate this work to my wife, Purity Nkirote, and our son, Noel Kimathi, for prayers, patience and encouragement during the entire study period. I will be grateful forever.

NOMENCLATURE

A = Lip pressure pipe area (cm^2);
c_f = Compressibility of the fluid (Pa^{-1});
c_t = Total compressibility of the water and rock (Pa^{-1});
c_r = Compressibility of the porous rock;
h = Reservoir thickness (m);
H_s = Saturated steam enthalpy at atmospheric pressure (kJ/kg);
H_t = Fluid enthalpy (kJ/kg);
H_w = Saturated water enthalpy at atmospheric pressure (kJ/kg);
k = Formation permeability (mD);
p = Reservoir pressure (Pa);
P_{lip} = Lip pressure (MPa);
Q = Volumetric flow rate (m^3/s);
Q_t = Total flow rate (kg/s);
Q_w = Water flow rate measured after separation in the silencer (kg/s) ;
r = Radial distance (m);
t = Time;
t_o = The time at circulation stop;
T = Transmissivity ($m^3/(Pa·s)$);
S = Storativity ($m^3/ (Pa.m^2)$);
Δt = Time passed since circulation stopped;
μ = Dynamic viscosity of the fluid (Pa·s);
ρ = Fluid density (kg/m^3) ;
φ = Porosity (%).

REFERENCES

Axelsson, G., 2008: Production capacity of geothermal systems. *Workshop for Decision Makers on Direct Heating Use of Geothermal Resources in Asia, Tianjin, China*. UNU-GTP, TBLRREM and TBGMED, CD, 14 pp.

Arason, Th., Björnsson, G., Axelsson, G., Bjarnason, J.Ö., and Helgason, P., 2003: *The geothermal reservoir engineering software package Icebox, user´s manual*. Orkustofnun, Reykjavík, manual, 53 pp.

Bw'Obuya, M. and Omenda, P., 2005: History of development of the conceptual model of Olkaria geothermal field by use of geophysics and other methods. In: Mwangi, M. (lecturer), *Lectures on Geothermal in Kenya and Africa*. UNU-GTP, Iceland, report 4, 15-27.

Earlougher, R.C., 1977: *Advances in well test analysis*. Soc. Petr. Eng., Monograph 5, 264 pp.

Grant, M.A., 1979: *Interpretation of downhole measurements in geothermal wells*. DSIR, Wellington, New Zealand, report 8, AMD-88, 66 pp.

Grant, M.A., Donaldson, I.G., and Bixley, P.F., 1982: *Geothermal reservoir engineering*. Academic Press, NY, 369 pp.

Horne, R.N., 1995: *Modern well test analysis, a computer aided approach* (2nd edition). Petroway Inc., USA, 257 pp.

Jónsson, P., 2010: *Injection well testing*. UNU-GTP, Iceland, unpublished lecture notes.

Júlíusson, E., Grétarsson, G., and Jónsson, P., 2008: *Well tester.1.0b. User´s guide*. ISOR - Iceland GeoSurvey, report 2008/63, 26 pp.

Kariuki, M.N., 2003: Reservoir assessment and wellbore simulations for the Olkaria Domes geothermal field, Kenya. Report 14 in: *Geothermal training in Iceland 2003*. UNU-GTP, Iceland, 337-360.

Lagat, J.K., 2004: *Geology, hydrothermal alteration and fluid inclusion studies of the Olkaria Domes geothermal field, Kenya.* University of Iceland, M.Sc. thesis, UNU-GTP, Iceland, report 1, 79 pp.

Odeny, O.N.J., 1999: Analysis of the downhole data and preliminary production capacity estimate for the Olkaria Domes geothermal field, Kenya. Report 11 in: *Geothermal training in Iceland 1999*. UNU-GTP, Iceland, 285-306.

Ofwona, C.O., 2002**:** *A reservoir study of Olkaria East geothermal system, Kenya*. University of Iceland, M.Sc. thesis, UNU-GTP, Iceland, report 1, 86 pp.

Omenda, P.A., 1998: The geology and structural controls of the Olkaria geothermal system, Kenya. *Geothermics, 27-1*, 55-74.

Opondo, K.M., 2007: *Corrosive species and scaling in wells at Olkaria and Reykjanes, Svartsengi and Nesjavellir, Iceland*. University of Iceland, M.Sc. thesis, UNU-GTP, Iceland, report 2, 73 pp.

Stefánsson, V., and Steingrímsson, B.S., 1990: *Geothermal logging I, an introduction to techniques and interpretation* (3rd edition). Orkustofnun, Reykjavík, report OS-80017/JHD-09, 117 pp.